Graphite morphologies from the Borrowdale deposit (NW England, UK): Raman and SIMS data

J. F. Barrenechea · F. J. Luque · D. Millward · L. Ortega · O. Beyssac · M. Rodas

Abstract Graphite in the Borrowdale (Cumbria, UK) deposit occurs as large masses within mineralized pipe-like bodies, in late graphite–chlorite veins, and disseminated through the volcanic host rocks. This occurrence shows the greatest variety of crystalline graphite morphologies recognized to date from a single deposit. These morphologies described herein include flakes, cryptocrystalline and spherulitic aggregates, and dish-like forms. Colloform textures, displayed by many of the cryptocrystalline aggregates, are reported here for the first time from any graphite deposit worldwide. Textural relationships indicate that spherulitic aggregates and colloform graphite formed earlier than flaky crystals. This sequence of crystallization is in agreement with the precipitation of graphite from fluids with progressively decreasing supersaturation. The structural characterization carried out by means of Raman spectroscopy shows that, with the exception of colloform graphite around silicate grains and pyrite within the host rocks, all graphite morphologies display very high crystallinity. The microscale SIMS study reveals light stable carbon isotope ratios for graphite ($\delta^{13}C = -34.5$ to $-30.2‰$), which are compatible with the assimilation of carbon-bearing metapelites in the Borrowdale Volcanic Group magmas. Within the main mineralized breccia pipe-like bodies, the isotopic signatures (with cryptocrystalline graphite being lighter than flaky graphite) are consistent with the composition and evolution of the mineralizing fluids inferred from fluid inclusion data which indicate a progressive loss of CO_2. Late graphite–chlorite veins contain isotopically heavier spherulitic graphite than flaky graphite. This agrees with CH_4-enriched fluids at this stage of the mineralizing event, resulting in the successive precipitation of isotopically heavier graphite morphologies. The isotopic variations of the different graphite morphologies can be attributed therefore, to changes in the speciation of carbon in the fluids coupled with concomitant changes in the XH_2O during precipitation of graphite and associated hydrous minerals (mainly epidote and chlorite).

Keywords Graphite · Morphology · Raman · Carbon isotopes · Borrowdale

J. F. Barrenechea · F. J. Luque (✉) · L. Ortega · M. Rodas
Departamento Cristalografía y Mineralogía, Facultad de Geología, Universidad Complutense de Madrid, 28040 Madrid, Spain
e-mail: jluque@geo.ucm.es

D. Millward
British Geological Survey, Murchison House, West Mains Road, Edinburgh EH9 3LA, UK

O. Beyssac
Laboratoire de Géologie, CNRS, Ecole Normale Supérieure, 24 rue Lhomond, 75005 Paris, France

Introduction

The graphite crystal structure consists of a continuous bidimensional array of sixfold rings of carbon atoms stacked along the *c*-axis. Thus, as for most other minerals with layered structures (e.g. phyllosilicates), the commonest habits of graphite are platy, flaky or scaly crystals (Kwiecinska 1980; Kavanagh and Schlogl 1988; Jaszczak 1995; Luque et al. 1998). However, in spite of its layered structure several other morphologies have been reported both in natural occurrences (rocks and meteorites) and in synthetic compounds (for instance, cast irons). Among these unusual graphite morphologies, the most common is

spherulites which may occur in many rock types (Gellatly 1966; Rumble et al. 1982; Duke and Rumble 1986; Katz 1987; Kvasnitsa et al. 1999; Doroshkevich et al. 2007), as a result of precipitation from fluids or melts. In addition, spherulitic graphite has also been found in some chondrites (e.g. Mostefaoui et al. 2000, 2005; El Goresy et al. 2005) and it is a common morphology developed in cast irons (Cooper et al. 2003; Östberg 2006; and references therein).

Fibrous (tubular) graphite has been found in artificially produced carbons (Jaszczak 1995) as well as in some meteorites (Mostefaoui et al. 2005) and igneous rocks (Jaszczak et al. 2007). Finally, other graphite morphologies including polyhedral (Gogotsi et al. 2000), columnar, pseudodipyramidal, pseudodipyramidal-prismatic (Kvasnitsa et al. 1999), and cone-shaped (Jaszczak et al. 2003, 2007) have been described.

The goal of the present paper is to describe the unique diversity of graphite morphologies occurring in a single paragenesis from the renowned epigenetic graphite deposit at Borrowdale in the English Lake District (Cumbria, UK; Fig. 1). The geological setting of this graphite deposit is also unusual, because it is one of only two known examples of graphite mineralization hosted by volcanic rocks (Barrenechea et al. 1997; Luque et al. 1998). Morphology of minerals is governed by crystalline structure and the physico-chemical conditions prevailing during nucleation and growth. Similarly, some geochemical features are also dependent upon the conditions of crystal growth. Thus, combining structural and isotopic characterization of the various graphite morphologies could help unravel the evolution of the mineralizing process in the particular environment of the volcanic-hosted deposit at Borrowdale, and more generally provide key information on graphite deposition from fluids.

Geological setting

The Borrowdale graphite deposit consists of mineralized faults hosted by andesite lavas and sills belonging to the upper Ordovician (Katian) Borrowdale Volcanic Group, and by a probably contemporaneous hypabyssal dioritic intrusion (Millward 2004) (Fig. 1). Previous geological studies of the deposit by Ward (1876) and Strens (1965) stated that narrow veins and stringers filling the faults comprise massive graphite and chlorite along with quartz.

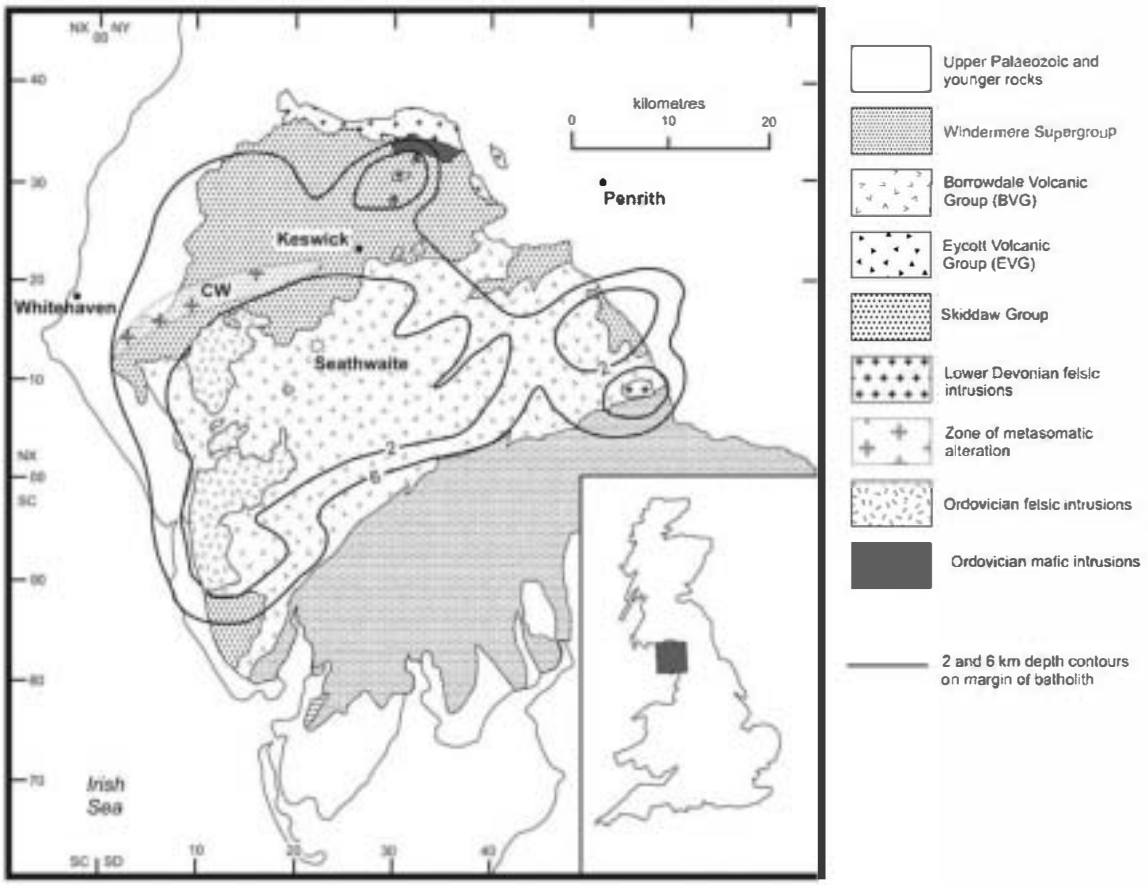

Fig. 1 Simplified geological map of the English Lake District (UK) locating the Borrowdale graphite deposit at Seathwaite. The bleached and metasomatically altered zone with the Skiddaw Group at Crummock Water (CW) is also shown

The richest deposits are developed at the intersections of the faults, where there are steeply inclined pipe-like bodies up to 1 × 3 m in cross-section and from a few metres to over 100 m in length (Ward 1876). The pipe-like bodies contain nodular masses and patches of graphite, typically 1–2 cm across, but ranging from a few millimetres to 1 m or more; the yellow–brown matrix comprises intensely altered wall-rock and brecciated quartz.

The volcanic rocks are underlain by the Skiddaw Group, a succession of marine turbiditic mudstones and sandstones, possibly late Cambrian to mid Ordovician in age, and at least 5,000 m thick (Cooper et al. 1995, 2004). Several lines of evidence suggest that Skiddaw Group rocks have contributed to the geochemical development of later aspects of Lake District geology. In particular, the presence of garnet phenocrysts in peraluminous rocks in the Borrowdale Volcanic Group and associated intrusions (Fitton 1972) has been attributed to the assimilation of pelitic material, most likely from the Skiddaw Group (McConnell et al. 2002). Sulfur isotope data from sulphides within these volcanic rocks also support this contention (Lowry et al. 1991). Preliminary data on the bulk carbon isotopic composition of carbonaceous matter disseminated within the Skiddaw metapelites are close to −28.5‰ (Barrenechea et al. 2008).

Analytical methods

Petrographic study

Samples from the graphite ore body and its host volcanic rocks were studied on polished thin sections with a Zeiss Axiophot microscope using both transmitted and reflected light. The recognition of graphite morphologies was complemented with the study of selected samples by scanning electron microscopy (SEM) on gold-coated fragments using a Jeol JSM6400 microscope operated at 40 kV.

Raman spectroscopy

Raman spectra were collected with a Renishaw INVIA spectrometer at the Ecole Normale Superieure (Paris, France) on the polished thin sections used for the petrographic study. This method allows for measurements in situ and for the preservation of the textural relationships between graphite and the rest of the minerals in the assemblage. All the measurements were done focusing the laser beam beneath the surface of transparent minerals (usually quartz, chlorite, and epidote) associated with graphite to avoid the mechanical disruption of the graphite structure at the surface of the thin section due to polishing (Pasteris 1989; Beyssac et al. 2003). The 514.5 nm wavelength of a 20 mW Spectra Physics Argon laser focused through a Leica DMLM microscope with a 100× objective (N.A. = 0.90) was used for the analyses. A 1,800 g/mm and a RENCAM CCD detector were used to disperse and analyze the signal.

Under these conditions the spatial resolution is ~1 μm and the spectral resolution is close to 1 cm^{-1}. Laser power on the sample surface was reduced to 2 mW to avoid radiation damage on graphite. Raman analysis of graphite might also be affected by polarization effects between the incident laser electromagnetic field and the structure of graphite. This effect might virtually enhance the defect bands especially for measurement on the graphite edge planes. These effects are rather weak with a 514.5 nm wavelength (Tan et al. 2004), and to further attenuate them we used a ¼ wavelength plate before the microscope which yields a circular polarization of the laser.

About 20 spectra of each type of graphite morphology were recorded to gain an insight into the structural heterogeneity within the sample. Acquisition time was 10 s and five accumulations ensured a good signal to noise ratio. No significant changes were observed in the second order Raman region of graphite, and thus the study focused on the first order Raman spectra (1,100–2,000 cm^{-1}). The Raman parameters (peak position, band area, and band intensity) were determined with the computer program PeakFit 3.0 using a Voigt function.

Stable carbon isotope analyses

Secondary ion mass spectrometry (SIMS) analyses were performed on the Cameca ims 1270 ion microprobe in the N.E.R.C. Scientific Services' Edinburgh Ion Microprobe Facility at the University of Edinburgh. Gold-coated polished thin sections were analyzed using negative secondary ions sputtered with a positively charged Cs^+ beam. The spot size was 20 μm. The results were checked using the graphite standard USGS24 ($\delta^{13}C = -16.05$‰; Coplen et al. 2006). Five measurements were made on the standard at the start and end of each 20 analyses—thus enabling calibration of the sample measurements against ten standard measurements. Under these conditions, the precision of the point analysis is close to 0.2‰. The $\delta^{13}C$ values are referred to the PDB standard.

Graphite morphologies

Graphite in the Borrowdale deposit occurs as subspherical to ellipsoidal aggregates (nodules hereafter) and as irregular patches or small veins within altered volcanic rocks of the Borrowdale Volcanic Group and in an associated hypabyssal dioritic intrusion. Nodules and patches may reach up to

10–15 cm in diameter or major length. Their typical size is 1–2 cm, though nodules up to 1 m have been recorded (Ward 1876; Fig. 2a). Graphite also occurs along fault planes in the volcanic rocks, usually associated with chlorite.

Graphite morphologies recognized within the nodules and patches are widely diverse and include both individual forms and aggregates (i.e. groups of individual forms; Table 1). Platy, flaky or scaly graphite crystals (up to 300 μm long and 50 μm wide) are by far the most abundant (≈90%), showing no preferred orientation relative to the margins of the nodules. Locally, composite nodules consisting of both flaky and cryptocrystalline graphite have been recognized (Fig. 2b), with flaky graphite usually surrounding cryptocrystalline graphite; the latter may form bands (i.e. colloform textures) around quartz fragments. In some nodules, thin coatings of flaky graphite on quartz fragments (termed hereafter as encapsulated fragments) have been recognized within cryptocrystalline graphite (Fig. 2c). In addition, cryptocrystalline graphite may form rounded patches within flaky graphite (Fig. 2d) and it also occurs with colloform textures, forming bands and globules dispersed within the host rock (Fig. 2e). Colloform graphite in the host rock can be observed around both silicate and pyrite grains (Fig. 2f).

Along with flaky and cryptocrystalline graphite two other morphological types have been recognized: spherulites and ring-like forms. Spherulites consist of radiating arrays of fibrous graphite crystals. In some cases, minute silicate grains can be observed forming the core of the spherulites. In the Borrowdale deposit, spherulites occur in four different settings: (1) as individual forms, 1–5 μm in diameter, or aggregates disseminated within the volcanic rock (Fig. 3a), (2) as individual forms, 5–40 μm in diameter, within flaky graphite (Fig. 3b), (3) as individual forms, 1–3 μm in diameter, enclosed in encapsulated quartz fragments (Fig. 2c), and (4) as aggregates, 5–10 μm in diameter, associated with chlorite along fault zones (Fig. 3c). Ring-like textures are usually hosted by cryptocrystalline graphite (Fig. 2c) or included within encapsulated fragments. Rings are 1–2 μm wide and consist of tiny graphite crystallites arranged parallel to both silicate and sulphide (mainly pyrite) cores.

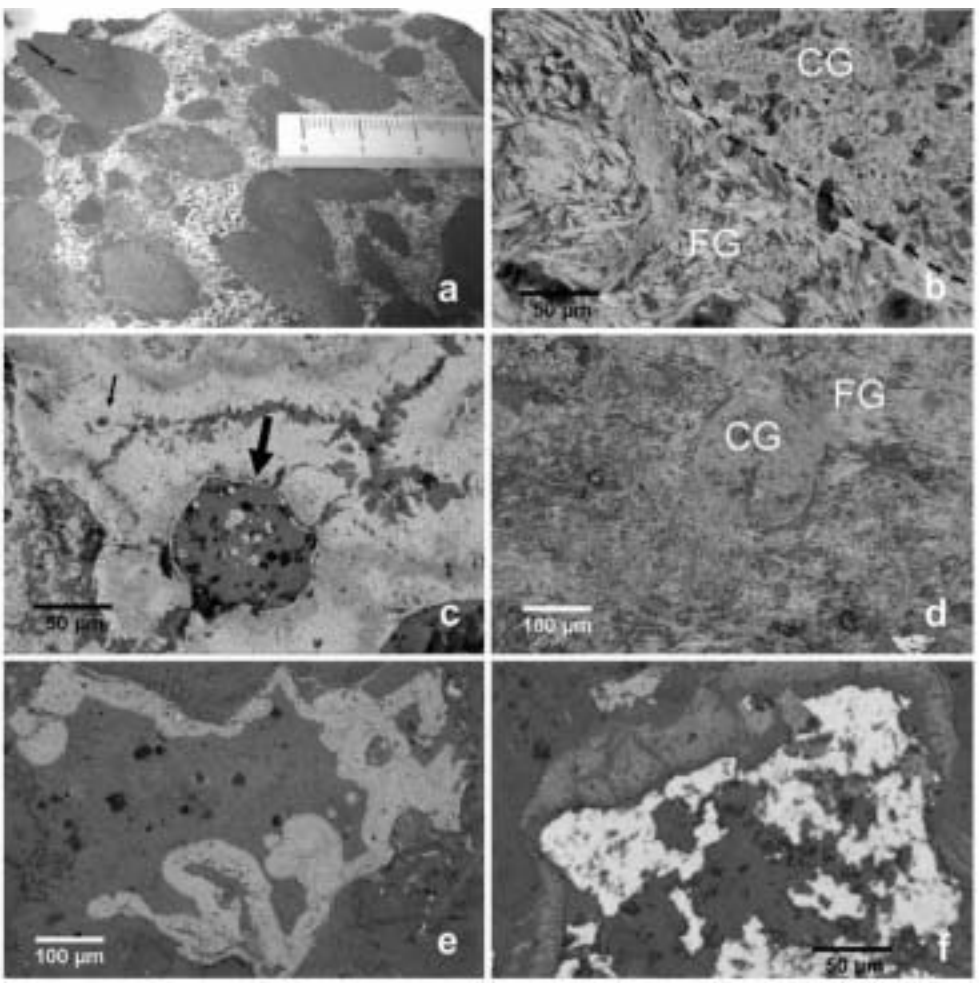

Fig. 2 Morphologies of graphite crystals and aggregates from the Borrowdale deposit. **a** Section of a hand sample showing the rounded to elliptical section of the graphite nodules within the altered andesite host rock. *Scale* is in centimeters. Photos (**b–f**) are reflected light photomicrographs (one polarizer). **b** Detail of the contact (*dashed line*) between flaky graphite (*FG*) and cryptocrystalline graphite (*CG*) in a composite nodule. **c** Large *arrow points* to an encapsulated quartz fragment (*dark grey*) with small graphite spherulites inside (*light grey*) embedded in cryptocrystalline (colloform) graphite; note the small graphite ring at the upper *left* corner of the photo (*small arrow*). **d** Rounded patch of cryptocrystalline graphite (*CG*) within flaky graphite (*FG*). **e** Colloform graphite (*light grey*) within the volcanic host rock; note reflectivity zoning parallel to the margins of the graphite aggregate. **f** Colloform graphite (*light grey*) around pyrite (*white*)

Table 1 Morphologies and characteristics of graphite from the Borrowdale deposit

Morphology	Occurrence	Host	Remarks
Aggregates			
Flaky, scaly	Nodules, irregular patches, coatings, disseminations	Altered andesite and diorite	Randomly distributed within nodules and patches (Fig. 2b)
Spherulitic	Patches	Chlorite	Individual size of spherulites ranging from 5 to 10 μm in diameter (Fig. 3c)
Cryptocrystalline	Patches, colloform	Altered andesite, flaky graphite (composite nodules)	Masses, bands and "globules" with apparent reflectance zoning (Figs. 2c–f, 5)
Individual forms			
Spherulites	Disseminations	Flaky graphite	5–40 μm in diameter (Fig. 3b)
Spherulites	Disseminations	Altered andesite	1–5 μm in diameter (Fig. 3a)
Spherulites	Disseminations	Encapsulated quartz fragments	1–3 μm in diameter (Fig. 2c)
Rings	Disseminations	Cryptocrystalline graphite, altered andesite	Nucleated on silicate or sulphide grains (Fig. 2c)
Flakes	Graphite–chlorite intergrowths	Chlorite	Thin curved and tapering crystals (Fig. 3d)
Vermicular	Graphite–chlorite intergrowths	Chlorite	Randomly distributed within chlorite (Fig. 3e)
Disks	Disseminations	Altered andesite	20–40 μm in diameter (Fig. 3f)

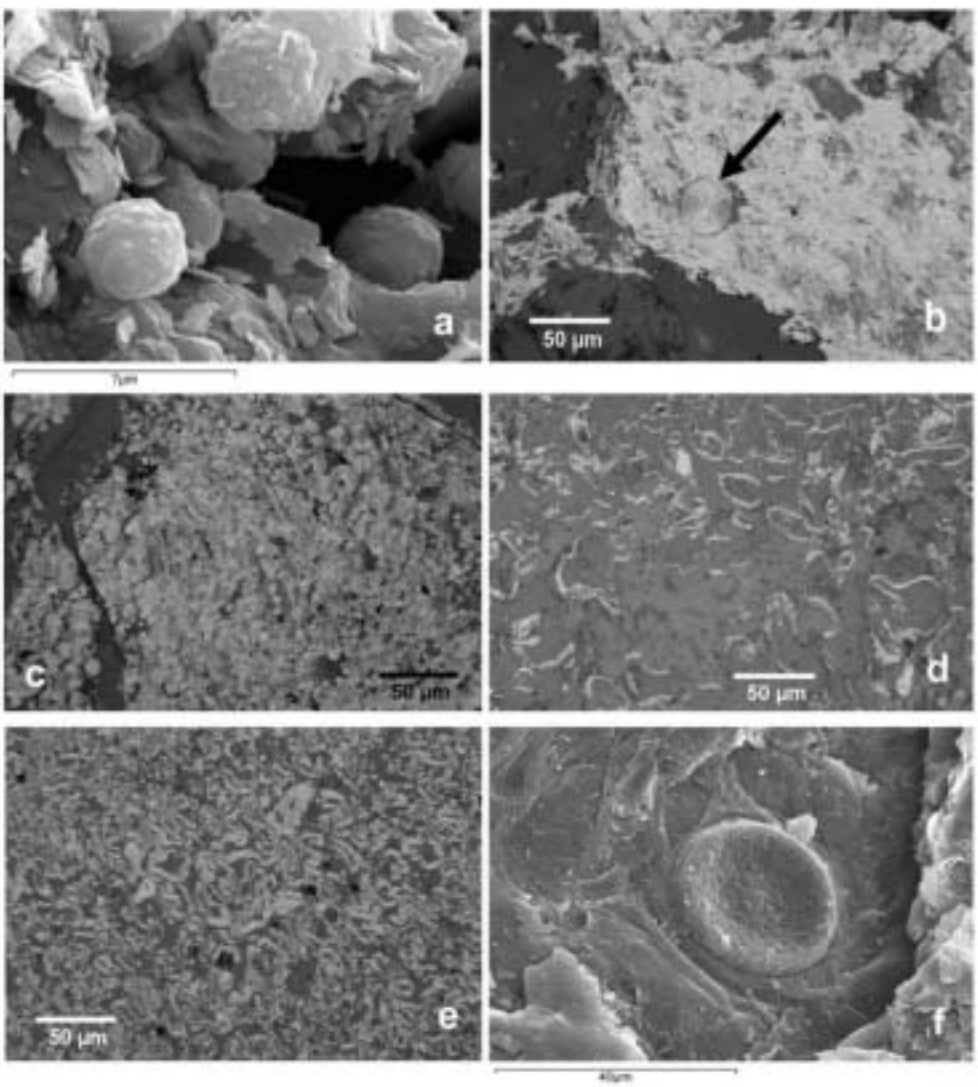

Fig. 3 Morphologies of graphite crystals and aggregates from the Borrowdale deposit. **a** Scanning electron microscope image of graphite spherulites disseminated within the volcanic host rock. Photos (**b–e**) are reflected light photomicrographs (one polarizer). **b** The *arrow points* to a graphite spherulite within flaky graphite. **c** Aggregate of graphite spherulites within chlorite. **d** Curved and tapering graphite flakes intergrown with chlorite. **e** Vermicular graphite intergrown with chlorite. **f** Scanning electron microscope image of dish-like graphite

Finally, "graphic-like" intergrowth textures, consisting of thin curved and tapering graphite flakes within chlorite (Fig. 3d), have been observed in samples from fault zones within the volcanic rock. In places, graphite in graphite-chlorite intergrowths shows a vermicular (i.e. worm-like) morphology (Fig. 3e).

In addition to these morphologies, the SEM study revealed the presence of concave disks (dish-shaped aggregates) of graphite (up to 40 μm in diameter) showing rough surfaces (Fig. 3f).

Raman data

The Raman spectra of graphite are sensitive to the changes in the degree of crystal perfection ("crystallinity") along the basal plane of the graphite structure (Wopenka and Pasteris 1993) that can be correlated to the in-plane crystallite size (L_a). Thus, the first order Raman spectra of highly crystalline graphite displays a sharp peak at ≈1,580 cm^{-1} (ordered or G band). Two additional bands at ≈1,350 and 1,620 cm^{-1} ($D1$ and $D2$ bands) are recorded in the first order Raman spectra of poorly crystalline graphite, the $D2$ band occurring as a shoulder on the G band. The intensity and area ratios for the disorder to order bands decrease with increasing crystallinity (Wopenka and Pasteris 1993; Beyssac et al. 2003). The most prominent feature in the second order Raman spectra of well-ordered graphite is a peak close to 2,700 cm^{-1} ($S1$ band) which splits into two bands. Recent detailed reviews of the physics behind the Raman spectrum of graphite are provided by Reich and Thomsen (2004) and Pimenta et al. (2007).

All graphite morphologies from the Borrowdale deposit correspond to structurally well ordered graphite according to the Raman data. The intensity and area ratios for the D and G bands in the first-order spectra are consistent with highly crystalline graphite. In addition, no significant changes were observed in the second order Raman region, all the spectra showing well-defined shoulders at ≈2,685 cm^{-1} on the $S1$-peak, which is indicative of the attainment of tri-periodic order in the structure (Lespade et al. 1982).

Flaky graphite

Raman spectra of flaky graphite from Borrowdale display a sharp G band and weak or absent $D1$ and $D2$ disorder bands (Fig. 4a). The intensity and area ratios for the disorder to order bands ($R1 = D1/G$ peak intensity ratio, and $R2 = D1/(G + D1 + D2)$ peak area ratio; Beyssac et al. 2002) average 0.04 for $R1$, and 0.06 for $R2$ (Table 2). These features of the Raman spectra indicate a high degree of crystalline perfection along the basal plane of the graphite structure. The average crystallite size L_a is in excess of 2,000 Å according to the estimation of Wopenka and Pasteris (1993) which is based on the area ratio of the $D1$ to G bands.

Cryptocrystalline graphite

Significant differences were observed in the first-order Raman spectra of cryptocrystalline graphite occurring in composite nodules in the pipe-like bodies compared with that found as colloform bands around silicate or sulphide grains within the volcanic host rocks (Table 2).

1. Cryptocrystalline graphite in composite nodules displays the Raman features of highly ordered graphite, that is, small or absent $D1$ peak and sharp G band (Fig. 4b). The average values for $R1$ and $R2$ are 0.09 and 0.05, respectively. Such values agree with in-plane crystallite sizes larger than 2,000 Å.
2. Colloform graphite around silicate grains in the volcanic host rock shows Raman spectra corresponding to graphite of lower crystallinity (Fig. 4c). In particular, the parameters of the first-order spectra $R1$ and $R2$ have higher average values (0.23 and 0.25, respectively) than those calculated for the other morphologies. Such values agree with L_a crystallite sizes of 200 to 300 Å.
3. Finally, the Raman spectra of colloform graphite around pyrite grains in the host rock (Fig. 4d) show the highest $R1$ and $R2$ average values (0.26 and 0.28, respectively) and hence the lowest degree of crystallinity (L_a = 150–300 Å).

Spherulitic graphite

The recorded Raman spectra of spherulitic graphite from the Borrowdale deposit also correspond to highly crystalline graphite (Fig. 4e). No differences have been found for spherulites disseminated in the host rocks or within encapsulated quartz fragments. The parameters of the first-order spectra $R1$ and $R2$ have average values of 0.07 and 0.06, respectively. Such values agree with average crystallite sizes larger than 2,000 Å. Graphite spherulites within flaky graphite were not analyzed because they can only be recognized at the surface of the polished thin sections.

Graphite in chlorite

Graphite (both flaky and vermicular) in "graphic"-like intergrowths and graphite spherulites within chlorite shows Raman spectra corresponding to well-ordered graphite

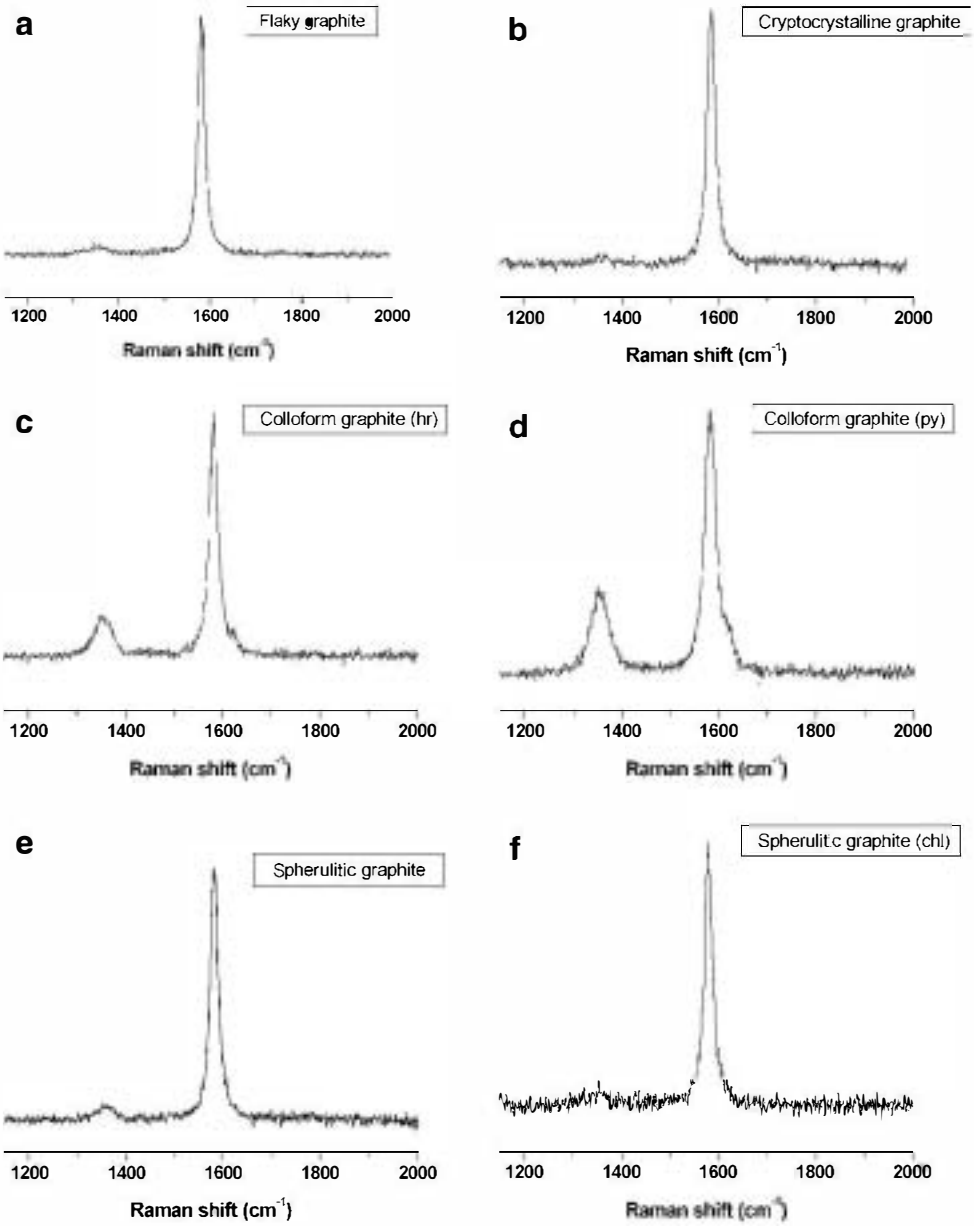

Fig. 4 First-order Raman spectra of the different graphite morphologies from the Borrowdale deposit. **a** Flaky graphite, **b** cryptocrystalline graphite from composite nodules, **c** colloform graphite surrounding silicate grains within the volcanic host rock (*hr*), **d** colloform graphite surrounding pyrite (*py*) within the volcanic host rock, **e** spherulitic graphite included in encapsulated quartz, **f** spherulitic graphite within chlorite (*chl*)

(Fig. 4f). However, *R*1 and *R*2 values are slightly higher than those for flaky and cryptocrystalline graphite within the nodules, and also compared to spherulitic graphite disseminated in the host rock or enclosed in encapsulated quartz fragments. The parameters of the first-order spectra *R*1 and *R*2 have average values of 0.11 and 0.16, respectively. Such values correspond to L_a crystallite sizes in the range between 1,000 and 1,500 Å.

Stable carbon isotope data

The stable carbon isotope ratios for the different morphologies analyzed are given in Table 3. No data were obtained for some of the morphologies because they were smaller than the spot size of the ion microprobe. It is worth noting that the analyses of each morphological type fall within very narrow ranges. The most abundant morphology within nodules and disseminations (flakes) has one of the heaviest isotopic signatures (average $\delta^{13}C_{PDB} = -30.26‰$) for the graphite in the deposit. Such values are close to those found in graphite spherulites within chlorite (average $\delta^{13}C_{PDB} = -30.15‰$). By contrast, cryptocrystalline graphite in composite nodules has significantly lighter isotopic signatures (average $\delta^{13}C_{PDB} = -33.70‰$) with no apparent zoning across the banded texture (Fig. 5). The lightest carbon isotope ratios correspond to vermicular graphite within chlorite (average $\delta^{13}C_{PDB} = -34.49‰$).

Table 2 Raman data for the different graphite morphologies

	G position (cm^{-1})	*D*1 position (cm^{-1})	*G* FWHM (cm^{-1})	*R*1	*R*2
Flaky					
Mean value	1,581	1,350	20	0.04	0.06
SD	1.2	2.5	2.9	0.09	0.09
Number of analyses	25				
Cryptocrystalline					
Mean value	1,581	1,355	21	0.09	0.05
SD	1.3	2.3	1.5	0.02	0.08
Number of analyses	17				
Spherulitic					
Mean value	1,582	1,356	20	0.07	0.06
SD	0.9	3.2	1.5	0.07	0.09
Number of analyses	15				
Colloform (silicate)					
Mean value	1,582	1,355	27	0.23	0.25
SD	1.7	2.8	2.5	0.09	0.09
Number of analyses	28				
Colloform (pyrite)					
Mean value	1,583	1,356	26	0.26	0.28
SD	1.0	2.4	2.2	0.08	0.07
Number of analyses	12				
Vermicular intergrowth (chlorite)					
Mean value	1,580	1,351	21	0.11	0.16
SD	1.3	3.0	1.5	0.06	0.07
Number of analyses	18				

G FWHM Full width at half maximum of the *G* band

Discussion

Origin of graphite morphologies

The variation in the morphology of minerals is related to factors influencing the growth forms. The theoretical morphology of a mineral, inferred from its structure, can be used as a reference to evaluate the influence of the different factors that affect its morphology in a certain setting. In the case of graphite, the structure is defined by layers of carbon atoms arranged parallel to the (0001) plane in a hexagonal crystalline lattice, ABAB stacking of aromatic planes (a rhombohedral polytype, ABCABC stacking, exists, as well but is very minor). Within these layers, strong covalent bonds exist. However, weak van der Waals forces keep the carbon layers together. The characteristics of this structure determine that (0001) surface exclusively cuts weak bonds. Therefore, this is a low attachment energy surface. By contrast, surfaces in the *c*-axis zone cut strong bonds and consequently have much higher attachment energies. It is well known that a direct relationship exists between the attachment energy of a surface and its growth rate, since the higher the attachment energy the faster the growth units attach onto it. Thus, any surface in the *c*-axis zone will grow much faster than the (0001) surface. Therefore, the expected habit for graphite crystals will be dominated by (0001) faces, whereas faces in the *c*-axis zone will have a very limited development, with the crystals showing a platy morphology.

Factors that can affect crystal growth must be considered in the interpretation of those graphite crystals showing morphologies that differ significantly from the theoretically expected one. The variation of graphite morphology can be attributed to (1) changes in the carbonaceous precursor, (2) the effect of elements other than carbon present in the environment, and (3) changes in the carbon content of the fluid. Thus, Mostefaoui et al. (2005) ascribed the various morphologies found in chondrites to different carbonaceous precursors. Such an assumption could be applied essentially to graphite in metamorphic rocks formed by graphitization of carbonaceous precursors in situ. However, graphite in metamorphic rocks occurs exclusively as flakes. On the other hand, it has been reported that in synthetic systems (i.e. cast irons) some elements (especially magnesium) promote the development of spherulitic graphite (Double and Hellawell 1995; Östberg 2006). This influence can be disregarded in natural (geological) systems because the usual concentrations of such elements in most rocks would

Table 3 Results of the ion probe analysis (SIMS) of graphite morphologies. The $\delta^{13}C$ values are relative to the PDB standard

Vermicular intergrowths in chlorite	$\delta^{13}C$ (‰)	Cryptocrystalline	$\delta^{13}C$ (‰)	Flakes	$\delta^{13}C$ (‰)
F2@1.asc	−34.87	P0@1.asc	−33.72	P0@17.asc	−29.26
F2@2.asc	−33.76	P0@2.asc	−32.56	P0@18.asc	−31.89
F2@3.asc	−33.99	P0@3.asc	−34.45	P0@19.asc	−28.97
F2@4.asc	−35.29	P0@5.asc	−34.09	P0@20.asc	−28.65
F2@5.asc	−34.20	P0@6.asc	−34.45	P0@21.asc	−29.72
F2@6.asc	−35.20	P0@7.asc	−33.87	P0@22.asc	−28.71
F2@7.asc	−35.15	P0@8.asc	−33.60		
F2@8.asc	−33.92	P0@9.asc	−31.60	G2C@1.asc	−30.85
F2@9.asc	−34.05	P0@10.asc	−32.10	G2C@2.asc	−31.31
		P0@11.asc	−34.29	G2C@3.asc	−30.56
Average	−34.49	P0@12.asc	−35.12	G2C@4.asc	−31.01
Standard deviation	0.62	P0@13.asc	−34.01	G2C@5.asc	−30.75
		P0@14.asc	−32.87	G2C@7.asc	−30.23
Spherulites in chlorite		P0@15.asc	−34.01	G2C@8.asc	−30.22
F2@11.asc	−29.87	P0@16.asc	−34.73	G2C@9.asc	−28.97
F2@12.asc	−30.02			G2C@10.asc	−31.55
F2@13.asc	−30.98	Average	−33.70	G2C@12.asc	−31.61
F2@14.asc	−29.76	Standard deviation	1.00		
F2@15.asc	−31.11			Average	−30.26
F2@16.asc	−29.18			Standard deviation	1.10
Average	−30.15				
Standard deviation	0.75				

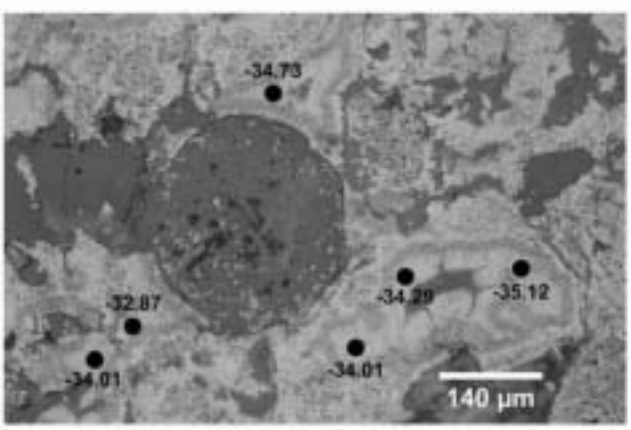

Fig. 5 Reflected light microphotograph (one polarizer) of a composite nodule showing the $\delta^{13}C$ values of cryptocrystalline (colloform) graphite. The points analyzed by SIMS are indicated by *small circles*

lead spherulitic graphite to be the most common morphology, and this does not actually occur. Thus, for fluid-deposited graphite occurrences, changes in the carbon content of the fluid (supersaturation) appear to be the most likely factor controlling the different graphite morphologies. In particular, unusually high supersaturation is required for graphite to be precipitated from moderate temperature fluids (Pasteris 1999), such as those responsible for the Borrowdale mineralization (Luque et al. 2009). High carbon concentrations also seem to play a key role in the development of graphite spherulites in carbonatite rocks. Spherulitic graphite in carbonatites, however, does not precipitate from a C–O–H fluid, but it crystallizes directly from the carbon-rich magma (Doroshkevich et al. 2007).

According to classical nucleation theory (Walton 1969), the number of critical nuclei that form in a system per unit time is an exponential function of the square of supersaturation. This explains why a large number of crystals reach a small size when nucleation occurs under high supersaturation conditions, while few large crystals are the result of nucleation under low supersaturation (Sunagawa 1987, 2005). Moreover, the formation of aggregates is also characteristic of crystallization from highly supersaturated fluids. The decrease in supersaturation during growth results in an evolution from cryptocrystalline and spherulitic aggregates to polyhedral crystals. If heterogeneous nucleation is considered and it occurs freely over any surface, various textures of polycrystalline aggregates will appear through geometrical selection. Spherulites will be formed on minute, nearly spherical grains during the early stages of nucleation, whereas cryptocrystalline aggregates displaying banding parallel to the substrate surface will nucleate and grow over

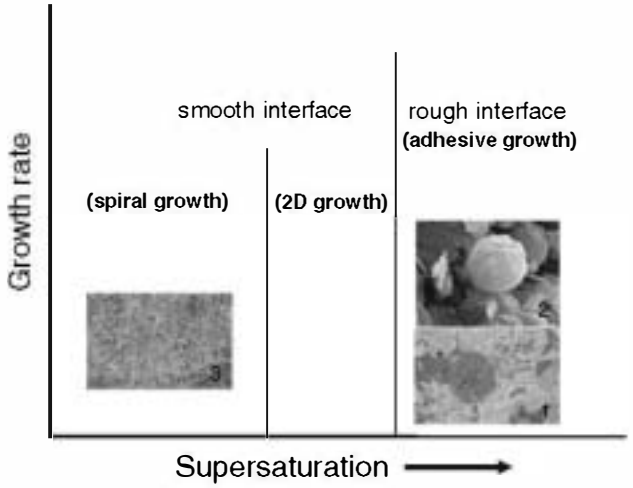

Fig. 6 Schematic diagram depicting the relationship between supersaturation and growth rate (based on Sunagawa 1987). The type of surface of aggregates and crystals and the nucleation mechanism prevailing in each field (in *brackets*) are shown. The images correspond to the three main graphite morphologies found in the Borrowdale deposit: *1* cryptocrystalline, *2* spherulitic, and *3* flaky

uneven substrate surfaces (colloform aggregates). Lower supersaturation favours the formation of polyhedral morphologies mainly by spiral growth (Fig. 6).

At high supersaturation conditions the solid–fluid interface becomes rough and crystal growth occurs by an adhesive or continuous mechanism. Under these conditions, growth is controlled by volume diffusion (Sunagawa 1987) and the resulting morphologies are much more elongated than those expected at lower supersaturation. If such elongate crystals grow radially around a minute nucleus, a spherulitic aggregate of acicular crystals will appear. In natural spherical graphite it has been shown that these spheres consist of an internal radial arrangement and a thin surface shell with concentric texture (see Jaszczak 1995). Such textures have been interpreted as the result of a conehelix growth mechanism from a common centre (Double and Hellawell 1974), which is the likely explanation of the origin of graphite spherulites in the Borrowdale deposit. In other cases, for example in marbles from Pargas (Finland), the surfaces of these spheres show outlines of individual graphite crystals with their basal planes lying parallel to the surface. These spheres are very similar to those found disseminated in the volcanic rocks of the Borrowdale deposit (compare Fig. 3a of this paper and 6–11 in Jaszczak 1995). This arrangement of the basal planes of graphite parallel to the substrate surface could also be responsible for the development of the ring-like textures observed (Fig. 2c).

Dish-like morphologies detected by SEM (Fig. 3f) are reported for the first time in this paper and they can be interpreted on the basis of structural considerations. As explained above, the (0001) surface is a low attachment energy surface while surfaces in the *c*-axis zone have higher attachment energies. Consequently, the growth units approaching faces in the *c*-axis zone attach onto them much more rapidly than onto (0001) face. Those faces that grow faster tend to disappear along the growth process. Moreover, when differences between the growth rates of faces in the same zone are at a minimum, curved surfaces or edges will develop. In addition, there is also a relationship between the surface energy of a face and its growth mechanism. Faces with high attachment energy values tend to be rough and grow by an adhesive or continuous mechanism. For dish-like graphite morphologies in the Borrowdale deposit, (0001) faces may have grown by two-dimensional nucleation, as they appear relatively flat and well developed, whereas those faces in the *c*-axis zone must have grown by a continuous mechanism, appearing as curved ledges (Fig. 3f).

Colloform aggregates of graphite were developed over irregular substrate surfaces starting from minute crystals of random orientation. After one layer is completed by intermittent growth, repetition of the process will develop the colloform texture. The interruption and resumption of growth inevitably occur in a system where there is an imbalance between the diffusion rate and the growth rate and a critical value such as the energy barrier is involved (Sunagawa 2005). During the early stage of growth, the particle size is small and there is a high density of nuclei resulting in cryptocrystalline aggregates displaying banded textures (colloform) parallel to the substrate surface (Figs. 2c, 5).

Finally, the most common morphology of graphite crystals (i.e. flaky) from the Borrowdale deposit would be developed under lower supersaturation conditions by spiral growth (Fig. 6). Each layer of the graphite structure can be considered as a two-dimensional sheet to which atoms can be added more easily in the in-plane directions than along the stacking direction, that is, the *c*-axis (normal to the layers). So, as expected from its structure, flakes will be the dominant morphology for graphite crystals in any natural system (both in metamorphic and fluid-deposited occurrences; Luque et al. 1998), and any other morphology would result from particular conditions during nucleation and growth. Textural relationships in the composite nodules from the Borrowdale deposit support the conclusion that flaky graphite crystallized later than those morphologies that formed under high supersaturation conditions (cryptocrystalline or spherulitic graphite; Figs. 2b, d, 3b).

Structural features of graphite morphologies

According to Raman data, graphite from the Borrowdale deposit is mainly well ordered. This is an unexpected feature considering that it was formed at relatively low

temperature (~500°C; Luque et al. 2009). Under the same analytical conditions, metamorphic graphite formed at equivalent temperatures (i.e. greenschist to epidote–amphibolite facies) distinctively shows a lower degree of order ($R1$ ratio ranging from 0.30 to 0.50, and average $R2$ close to 0.45; Beyssac et al. 2002) than that estimated in this study of the Borrowdale deposit. Compared with metamorphic graphite, the $R1$ and $R2$ ratios of the Raman spectra for the Borrowdale graphite (except for colloform graphite surrounding silicate or sulphide grains in the volcanic host rock) are in the range for graphite occurring at high-grade metamorphic conditions, from upper amphibolite to granulite facies rocks (Pasteris and Wopenka 1991; Wopenka and Pasteris 1993; Beyssac et al. 2002). Thus, the Borrowdale deposit represents the first example of fully ordered graphite in a large graphite occurrence precipitated from fluids at moderate temperature. The reasons for such an anomalous crystallinity are discussed in detail in a previous paper (Luque et al. 2009) and can be summarized as: (1) the different mechanism of formation for fluid-deposited graphite compared with metamorphic graphite, the latter being the progressive transformation in situ of a carbonaceous precursor, (2) the stability field for fully ordered graphite + fluid in the C–O–H system is larger than that for poorly ordered graphite even at relatively low temperatures, (3) the heterogeneous nucleation mechanism operating during graphite deposition that reduced the energy barrier for graphite precipitation from the fluid, and (4) the fluids responsible for the Borrowdale mineralization had the very high initial concentration of carbon required for the precipitation of graphite from such moderate temperature fluids.

Considering the overall high crystallinity of graphite in the deposit, an explanation of the lower crystallinity displayed by the cryptocrystalline graphite in the colloform textures around pyrite and silicate grains within the volcanic host rock is required. Colloform graphite around pyrite shows the lowest crystallinity, with average in-plane crystallite sizes ranging from 150 to 300 Å. The catalytic effect of certain compounds on the precipitation of graphite, particularly sulphides (pyrrhotite, stibnite), is well known (Jedwab and Boulegue 1984; Duke and Rumble 1986). Silicates also have been proposed as catalytic agents during the graphitization of carbonaceous matter through metamorphism (Grew 1974). So, it is likely that the increased rate of graphite precipitation caused by these catalysts induced some kind of disorder in the graphite structure. However, it is worth noting that colloform graphite around quartz in composite nodules within the mineralized bodies and colloform graphite around silicates in the volcanic host rocks have contrasting crystallinities. Colloform graphite around quartz has L_a values in excess of 2,000 Å, whilst colloform graphite around silicates in the volcanic host rocks has L_a = 200–300 Å. Thus, it seems likely that ferromagnesian minerals within the host rock caused a similar effect to that of pyrite, whereas quartz does not appear to influence any structural disorder in the precipitated graphite.

As with cryptocrystalline graphite, graphite spherulites also developed under high supersaturation conditions. Raman parameters measured on spherulitic graphite within nodules from the mineralized bodies indicate a high degree of ordering, similar to that found in graphite from high-grade metamorphic rocks, with L_a larger than of 2,000 Å. In addition, graphite spherulites in the chlorite–graphite veins also have large L_a crystallite sizes (>1,000 Å). Previous Raman data on graphite spherulites both in synthetic systems (cast irons) and natural occurrences (chondrite meteorites and carbonatites) point to poorly crystalline materials. Cooper et al. (2003) reported Raman spectra from spherulitic graphite in cast irons showing intense $D1$ and $D2$ peaks that reveal low crystallinity. Mostefaoui et al. (2000) found spherulitic graphite in primitive chondrites with L_a between 30 and 40 Å. Similarly, Doroshkevich et al. (2007) reported graphite spherulites in carbonatites with $R1$ in the range 0.35–0.84. The large difference in crystallinity between graphite spherulites in cast irons and carbonatites, and those found in Borrowdale can be interpreted as a consequence resulting from an unlikely analytical procedure. In both the cast irons and carbonatites, the Raman measurements were done on polished surfaces and the polishing process appears to be the cause of such a low crystallinity. The Raman spectra on graphite spherulites in chondrites were obtained over unpolished surfaces, so a different argument should be invoked to explain its low crystallinity. Graphite in chondrites results from heating of carbonaceous precursors at high temperatures (>1,000°C) for a very short period of time, with no pressure contribution (Mostefaoui et al. 2000). Such conditions are similar to those of experimental graphitization (Beny-Bassez and Rouzaud 1985) in which the products displayed Raman spectra corresponding to poorly crystalline graphite. Thus, the very different crystallinity of graphite spherulites in chondrites compared with those from Borrowdale should be attributed to their contrasting mechanisms of formation.

Significance of the carbon isotope ratios

In a first approach, stable carbon isotope ratios in graphite provide information about the origin of the carbon. For fluid-deposited graphite, the possible sources of carbon are (1) devolatilization of carbonaceous metapelites, (2) decarbonation of carbonate rocks, and (3) mantle-derived carbon (Luque et al. 1998). Each source has carbon isotope ratios falling within characteristic ranges. The total range

of $\delta^{13}C$ values for organic matter (both living and dead) is from about −40 to +6‰, with an average $\delta^{13}C$ value of −25‰; that is, organic materials are isotopically light (Weis et al. 1981). Marine carbonates of Cambrian to Tertiary age, on the other hand, have heavier $\delta^{13}C$ values which lie within ± 2 units of 0‰. The isotopic compositions of diamonds and mid-oceanic ridge basalts (MORB) indicate that carbon from the mantle is significantly heavier ($\delta^{13}C = -7$‰) than biogenically derived carbon (Crespo et al. 2006).

The interpretation of the carbon isotopic signature in terms of the carbon source is complicated by fractionation effects related to the thermal history of the rock or to carbon-exchange between graphite and other carbon-bearing species, such as an isotopically heavier carbonate (which in turn is also governed by temperature). In the fractionation that occurs between two phases, the more oxidized species of the pair becomes relatively enriched in the heavier isotope, i.e. ^{13}C. In the maturation of organic matter, fractionation occurs between organic residues and their evolved gas species. For a fluid co-existing with the FQM buffer, the fluid becomes richer in the oxidized species (CO_2) with increasing temperature (Frost 1979). Thus, at low temperature and under low fO_2 conditions, co-existing CH_4 becomes depleted in ^{13}C, giving the gas an isotopically lighter signature and the residual carbonaceous matter a heavier one (Bottinga 1969). At relatively high fO_2 the carbon-bearing species resulting from devolatilization of carbonaceous matter would be an isotopically light CO_2, but heavier than the residual carbonaceous matter. The decarbonation reactions of carbonate minerals result in a ^{13}C-enriched CO_2 phase. Incorporation of such CO_2 into aqueous fluids would lead to the precipitation of isotopically heavy graphite. Finally, the possibility of mixing between different carbon reservoirs before or while graphite precipitated from the fluid should be also considered when interpreting the carbon isotopic signature of fluid-deposited graphite (see Luque et al. 1998).

The light isotopic signatures of the different morphologies of graphite from the Borrowdale deposit suggest that the carbon was derived from a biogenic source. This is in good agreement with the geological and geochemical evidence of assimilation of Skiddaw Group metapelites by the volcanic host rocks, and with the presence of zones within the metapelites that have been depleted in carbon and other elements during hydrothermal alteration (e.g. the Crummock Water zone, Fig. 1; Cooper et al. 1988). As previously mentioned, the bulk carbon isotopic analyses of Skiddaw metapelites yielded values close to $\delta^{13}C = -28.5$‰. Considering the solidus temperature of andesite magmas, the assimilation of the Skiddaw metapelites should occur at temperatures close to 1,100°C. At such temperature the released carbon species is CO_2, and the fractionation factor C–CO_2 is about 5.5‰ (Scheele and Hoefs 1992). Thus, the $\delta^{13}C$ value for the CO_2 at the assimilation temperature was close to −23‰. At the temperature estimated for graphite precipitation (480–500°C; Luque et al. 2009), the fractionation factors for CO_2–C would be close to 10.5‰ (Bottinga 1969). This means that the graphite precipitated from this CO_2-rich fluid should have an isotopic signature close to −33.5‰.

Fluid inclusion data in the Borrowdale deposit (Ortega et al. 2008; Luque et al. 2009) have shown that fluids involved in the mineralizing process had average compositions of 0.65 mol fraction H_2O and $XCO_2/(XCO_2 + XCH_4) = 0.69$ in the main stage of graphite precipitation. Later, the fluids evolved towards 0.93 mol fraction H_2O and $XCO_2/(XCO_2 + XCH_4) = 0$, with CH_4 being the only carbonic species in the fluid in the final stages of fluid circulation. The graphite-mineralizing fluid would be a vapour-like supercritical phase at the beginning of the graphite precipitation, evolving to a liquid-rich fluid as the deposition proceeded. The conspicuous relationship between epidote and graphite in the breccia pipe-like bodies strongly suggests that the graphite precipitation started following the reaction $CO_2 \rightarrow C + O_2$. Since the average XCO_2 in the early fluid is 0.24 and epidote is not stable for $XCO_2 > 0.2$ (Liou 1993), epidote crystallization was likely triggered by the consumption of CO_2 in the reaction of graphite precipitation. The earlier morphologies (colloform) crystallizing in the pipe-like bodies display lighter signatures ($\delta^{13}C = -33.7$‰) than flaky graphite ($\delta^{13}C = -30.2$‰) that formed somewhat later. The values for cryptocrystalline graphite forming colloform textures in the composite nodules has therefore isotopic signatures similar to that of graphite crystallizing from CO_2 in the fluid with an initial $\delta^{13}C$ around −23‰. Flaky graphite is on average 3.5‰ heavier than colloform graphite within the main mineralized bodies, and this can be ascribed to CO_2 consumption in the fluid. It has been documented that changes in the CO_2/CH_4 ratio in the fluid may result in relatively large isotopic shifts. Such variations in the CO_2/CH_4 ratio can be also influenced by changes in the XH_2O, for example, by hydration reactions occurring simultaneously with graphite deposition (Duke and Rumble 1986).

Fluid inclusion data reveal a progressive enrichment in water as graphite mineralization proceeded, pointing to the involvement of water-generating reactions during graphite deposition: (1) $CH_4 + O_2 \rightarrow C + 2H_2O$ or (2) $CH_4 + CO_2 \rightarrow 2C + 2H_2O$ (or both). The reaction between CH_4 and CO_2 to form graphite is kinetically very sluggish, so reaction (1) seems to be more likely to account for graphite deposition in a later stage of the mineralizing event. The simultaneous consumption of CH_4 and water enrichment in the fluid drove its composition along the graphite saturation curve towards the CO_2-rich side, resulting in an isotopic

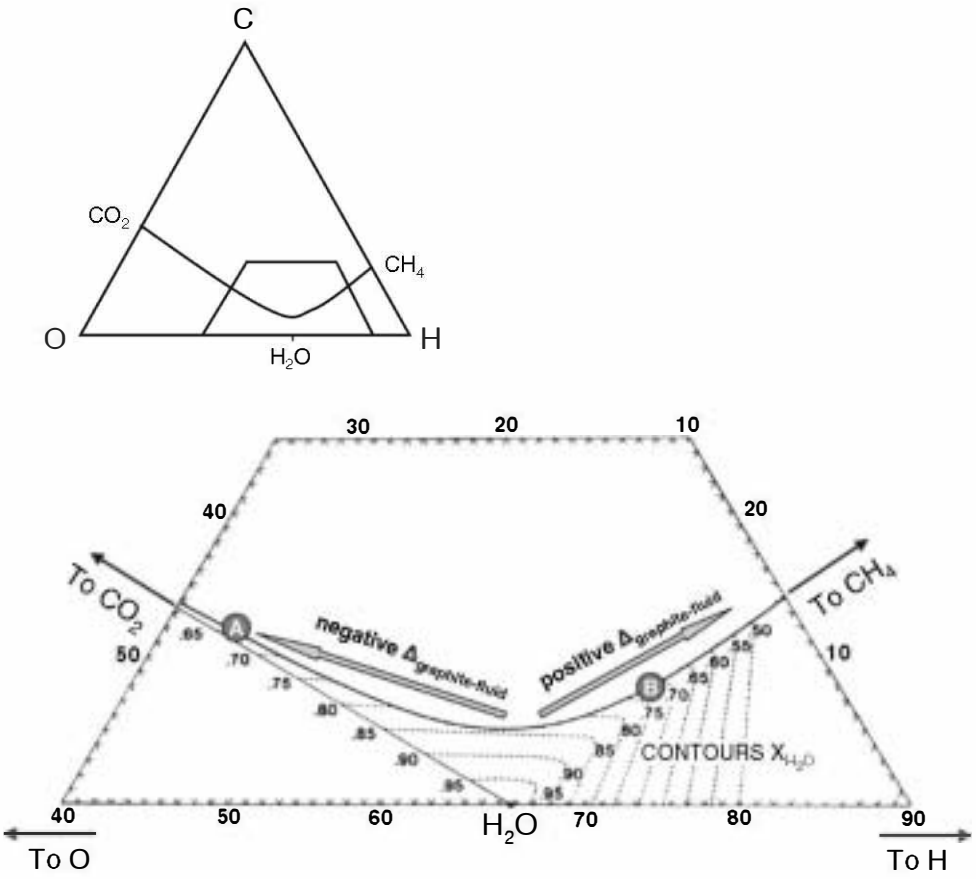

Fig. 7 Phase diagram of the C–O–H system at 600°C and 3.5 kbar showing the graphite-fluid isotopic fractionation as a function of fluid composition (modified after Duke and Rumble 1986). Along the graphite saturation curve, for CO_2-rich fluids (like fluid *A* in the graph), CO_2-depletion and/or H_2O-enrichment will result in the precipitation of isotopically heavier graphite. The first mineralizing fluids in the Borrowdale deposit were similar in composition to fluid A (Luque et al. 2009). Conversely, CH_4-depletion and/or water enrichment in CH_4-rich fluids (like fluid *B*) will cause the precipitation of isotopically lighter graphite. These qualitative variations of $\Delta_{graphite\text{-}fluid} = \delta^{13}C_{graphite} - \delta^{13}C_{fluid}$ are relatively insensitive to the exact temperature chosen for the system (Duke and Rumble 1986). For explanation see text

shift towards lighter $\delta^{13}C$ values in the precipitated graphite (Fig. 7). In this way, the isotopic signature of vermicular graphite ($\delta^{13}C = -34.5‰$) in graphite–chlorite assemblages from fault-fills would be lighter than that of the earlier formed spherulitic graphite ($\delta^{13}C = -30.2‰$). This suggests, though does not prove, that graphite–chlorite veins represent a slightly later mineralizing phase involving deposition from fluids in which the dominant carbonic species became CH_4. The variations in the $\delta^{13}C$ values between the different graphite morphologies (both in the pipes and in the graphite–chlorite veins) can be explained therefore through a Rayleigh distillation mechanism from an initial CO_2–CH_4–H_2O single fluid promoting graphite precipitation over a narrow (nearly isothermal) temperature interval. This interpretation is consistent with the evolution of the composition of the fluid obtained from fluid inclusion data and agrees with the morphology of the mineralized bodies (pipe-like breccias) which indicates a rapid, catastrophic mineralizing event.

Conclusions

Graphite in the Borrowdale (Cumbria, UK) deposit occurs as large masses within mineralized pipe-like bodies, as late graphite–chlorite veins, and disseminated through its andesite and dioritic host rocks. Graphite from Borrowdale shows the greatest variety of crystalline morphologies recognized up to now from a single deposit. In addition to flaky crystals, graphite also occurs as cryptocrystalline aggregates displaying colloform textures (reported for the first time in any graphite deposit worldwide), as spherulitic aggregates, and with dish-like morphologies. Colloform graphite occurs around silicate (both ferromagnesian minerals of the volcanic host rock and quartz within the breccia pipe mineralized body) and sulphide (mainly pyrite in the host rock) substrates. Textural relationships indicate that spherulitic aggregates and colloform textures are earlier than flaky crystals. This sequence of crystallization is related to the precipitation of graphite from fluids with progressively decreasing supersaturation.

With the exception of colloform graphite around silicate and pyrite grains within the host rocks, all graphite morphologies display very high crystallinity, as revealed by their in-plane crystallite sizes. Such high crystallinity is unusual for moderate temperature fluid-deposited graphite and this has been discussed in detail in a previous paper (Luque et al. 2009). The lower crystallinity of colloform graphite within the host rock is attributed to the structural

disorder induced by the catalytic effect of ferromagnesian and sulphide minerals during crystallization.

The light stable carbon isotope ratios of graphite ($\delta^{13}C = -34.5$ to $-30.2‰$) are compatible with the assimilation of carbon-bearing metapelites in the Borrowdale Volcanic Group magmas. In the main mineralized breccia pipe-like bodies, the microscale isotopic signatures (with cryptocrystalline graphite being lighter than flaky graphite) are consistent with the composition and evolution of the mineralizing fluids which indicate a progressive loss of CO_2 (from precipitation of graphite through the reaction $CO_2 \rightarrow C + O_2$). Late graphite–chlorite veins contain isotopically heavier spherulitic graphite than flaky graphite. This agrees with the fact that the fluids, as evidenced from fluid inclusion data, were richer in CH_4 at this stage of the mineralizing event, resulting in the successive precipitation of isotopically heavier graphite morphologies. The dominant graphite-producing reaction at this stage was $CH_4 + O_2 \rightarrow C + 2H_2O$. Thus, the isotopic variations of the different graphite morphologies can be attributed to changes in the speciation of carbon in the fluids coupled with concomitant changes in the XH_2O during precipitation of graphite and associated hydrous minerals (mainly epidote and chlorite).

References

Barrenechea JF, Luque FJ, Rodas M, Pasteris JD (1997) Vein-type graphite mineralization in the Jurassic volcanic rocks of the external zone of the Betic Cordillera (Southern Spain). Can Mineral 35:1379–1390

Barrenechea JF, Luque FJ, Ortega L, Rodas M, Millward D, Beyssac O (2008) Graphite morphologies in the volcanic-hosted deposit at Borrowdale (NW England, UK): preliminary Raman and SIMS data. Macla 9:91–92

Beny-Bassez C, Rouzaud J-N (1985) Characterization of carbonaceous materials by correlated electron optical microscopy and Raman microspectroscopy. Scan Electron Microsc 1985:119–132

Beyssac O, Goffé B, Chopin C, Rouzaud J-N (2002) Raman spectra of carbonaceous materials in metasediments: a new geothermometer. J Metamorphic Geol 20:859–871

Beyssac O, Goffé B, Petitet JP, Froigneux E, Moreau M, Rouzaud J-N (2003) On the characterization of disordered and heterogeneous carbonaceous materials by Raman spectroscopy. Spectrochim Acta A Mol Biomol Spectrosc 59:2267–2276. doi:10.1016/S1386-1425(03)00070-2

Bottinga Y (1969) Calculated fractionation factors for carbon and hydrogen isotope exchange in the system calcite–carbon dioxide–graphite–methane–hydrogen–water vapor. Geochim Cosmochim Acta 33:49–64. doi:10.1016/0016-7037(69)90092-1

Cooper DC, Lee MK, Fortey NJ, Cooper AH, Rundle CC, Webb BC, Allen PM (1988) The Crummock water aureole: a zone of metasomatism and source of ore metals in the English Lake District. J Geol Soc London 145:523–540. doi:10.1144/gsjgs.145.4.0523

Cooper AH, Rushton AWA, Molyneux SG, Hughes RA, Moore RM, Webb BC (1995) The stratigraphy, correlation, provenance and paleogeography of the Skiddaw Group (Ordovician) in the English Lake District. Geol Mag 132:185–211

Cooper CA, Elliot R, Young RJ (2003) Investigation of the graphitic microstructure in flake and spheroidal cast irons using Raman spectroscopy. J Mater Sci 38:795–802. doi:10.1023/A:1021813115611

Cooper AH, Fortey NJ, Hughes RA, Molyneux SG, Moore RM, Rushton AWA, Stone P, Allen PM, Cooper DC, Evans JA, Hirons SR, Webb BC (2004) The Skiddaw Group of the English Lake District. Memoir of the British Geological Survey. HMSO, London

Coplen TB, Brand WA, Gehre M, Gröning M, Meijer HAJ, Toman B, Verkouteren RM (2006) New guidelines for $\delta^{13}C$ measurements. Anal Chem 78:2439–2441. doi:10.1021/ac052027c

Crespo E, Luque J, Rodas M, Wada H, Gervilla F (2006) Graphite–sulfide deposits in Ronda and Beni Bousera peridotites (Spain and Morocco) and the origin of carbon in mantle-derived rocks. Gondwana Res 9:279–290. doi:10.1016/j.gr.2005.10.003

Doroshkevich AG, Wall F, Ripp GS (2007) Magmatic graphite in dolomite carbonatite at Pogranichnoe, North Transbaikalia, Russia. Contrib Mineral Petrol 153:339–353. doi:10.1007/s00410-006-0150-z

Double DD, Hellawell A (1974) Cone-helix growth forms of graphite. Acta Metall 22:481–487. doi:10.1016/0001-6160(74)90101-1

Double DD, Hellawell A (1995) The nucleation and growth of graphite: the modification of cast iron. Acta Metall Mater 43:2435–2442. doi:10.1016/0956-7151(94)00416-1

Duke EF, Rumble D (1986) Textural and isotopic variations in graphite from plutonic rocks, South-Central New Hampshire. Contrib Miner Petrol 93:409–419. doi:10.1007/BF00371711

El Goresy A, Zinner E, Pellas P, Caillet C (2005) A menagerie of graphite morphologies in the Acapulco meteorite with diverse carbon and nitrogen isotopic signatures: implications for the evolution history of acapulcoite meteorites. Geochim Cosmochim Acta 69:4535–4556. doi:10.1016/j.gca.2005.03.051

Fitton JG (1972) The genetic significance of almandine–pyrope phenocrysts in the calc-alkaline Borrowdale Volcanic Group, northern England. Contrib Miner Petrol 36:231–248. doi:10.1007/BF00371434

Frost BR (1979) Mineral equilibria involving mixed-volatiles in a C–O–H fluid phase: the stabilities of graphite and siderite. Am J Sci 279:1033–1059

Gellatly DC (1966) Graphite in natural and experimental carbonate systems. Min Mag (Lond) 35:963–970. doi:10.1180/minmag.1966.035.275.08

Gogotsi Y, Libera JA, Kalashnikov N, Yoshimura M (2000) Graphite polyhedral crystals. Science 290:317–320. doi:10.1126/science.290.5490.317

Grew ES (1974) Carbonaceous materials in some metamorphic rocks of New England and other areas. J Geol 82:50–73

Jaszczak JA (1995) Graphite: flat, fibrous and spherical. In: Mendenhall GD (ed) Mesomolecules: from molecules to materials. Chapman and Hall, London

Jaszczak JA, Robinson GW, Dimovski S, Gogotsi Y (2003) Naturally occurring graphite cones. Carbon 41:2085–2092. doi:10.1016/S0008-6223(03)00214-8

Jaszczak JA, Dimovski S, Hackney SA, Robinson GW, Bosio P, Gogotsi Y (2007) Micro- and nanoscale graphite cones and tubes from Hackman Valley, Kola Peninsula, Russia. Can Mineral 45:379–389. doi:10.2113/gscanmin.45.2.379

Jedwab J, Boulegue J (1984) Graphite crystals in hydrothermal vents. Nature 310:41–43. doi:10.1038/310041a0

Katz MB (1987) Graphite deposits of Sri Lanka: a consequence of granulite facies metamorphism. Miner Depos 22:18–25. doi:10.1007/BF00204238

Kavanagh A, Schlogl R (1988) The morphology of some natural and synthetic graphites. Carbon 26:23–32. doi:10.1016/0008-6223(88)90005-X

Kvasnitsa VN, Yatsenko VG, Jaszczak JA (1999) Disclinations in unusual graphite crystals from anorthosites of Ukraine. Can Mineral 37:951–960

Kwiecinska B (1980) Mineralogy of natural graphites. Polska Akad Nauk Prace Miner 67:5–79

Lespade P, Al-Jishi R, Dresselhaus MS (1982) Model for Raman scattering from incompletely graphitized carbons. Carbon 20:427–431. doi:10.1016/0008-6223(82)90043-4

Liou JG (1993) Stabilities of natural epidotes. In: Hock V and Koller F (eds). Proc 125 Jahre Kappenwand symposium, pp 7–16

Lowry D, Boyce AJ, Pattrick RAD, Fallick AE, Stanley CJ (1991) A sulphur isotopic investigation of the potential sulphur sources for Lower Palaeozoic-hosted vein mineralization in the English Lake District. J Geol Soc London 148:993–1004. doi:10.1144/gsjgs.148.6.0993

Luque FJ, Pasteris JD, Wopenka B, Rodas M, Barrenechea JF (1998) Natural fluid-deposited graphite: mineralogical characteristics and mechanisms of formation. Am J Sci 298:471–498

Luque FJ, Ortega L, Barrenechea JF, Millward D, Beyssac O, Huizenga J-M (2009) Deposition of highly crystalline graphite from moderate-temperature fluids. Geology (in press)

McConnell BJ, Menuge JF, Hertogen J (2002) Andesite petrogenesis in the Ordovician Borrowdale Volcanic Group of the English Lake District by fractionation, assimilation and mixing. J Geol Soc London 159:417–424. doi:10.1144/0016-764901-114

Millward D (2004) The Caradoc volcanoes of the English Lake District. Proc Yorks Geol Soc 55:73–105

Mostefaoui S, Perron C, Zinner E, Sagon G (2000) Metal-associated carbon in primitive chondrites: structure, isotopic composition, and origin. Geochim Cosmochim Acta 64:1945–1964. doi:10.1016/S0016-7037(99)00409-3

Mostefaoui S, Zinner E, Hoppe P, Stadermann FJ, El Goresy A (2005) In situ survey of graphite in unequilibrated chondrites: morphologies, C, N, O and H isotopic ratios. Meteorit Planet Sci 40:721–743

Ortega L, Luque J, Barrenechea JF, Millward D, Beyssac O, Huizenga J-M, Rodas M (2008) Fluid composition and reactions of graphite precipitation in the volcanic-hosted deposit at Borrowdale (NW England): evidence from fluid inclusions. Macla 9:177–178

Östberg G (2006) Perspectives on research on the formation of nodular graphite in cast iron. Mater Des 27:1007–1015

Pasteris JD (1989) In situ analysis in geological thin-sections by laser Raman microprobe spectroscopy: a cautionary note. App Spectr 43:567–570. doi:10.1366/0003702894202878

Pasteris JD (1999) Causes of the uniformly high crystallinity of graphite in large epigenetic deposits. J metamorphic Geol 17:779–787

Pasteris JD, Wopenka B (1991) Raman spectra of graphite as indicators of degree of metamorphism. Can Mineral 29:1–9

Pimenta MA, Dresselhaus G, Dresselhaus MS, Cancado LG, Jorio A, Saito R (2007) Studying disorder in graphite-based systems by Raman spectroscopy. Phys Chem Chem Phys 9:1276–1291. doi:10.1039/b613962k

Reich S, Thomsen C (2004) Raman spectroscopy of graphite. Philos Trans R Soc Lond A 362:2271–2288. doi:10.1098/rsta.2004.1454

Rumble D, Ferry JM, Hoering TC, Boucot AJ (1982) Fluid flow during metamorphism at the Beaver Brook fossil locality, New Hampshire. Am J Sci 282:886–919

Scheele N, Hoefs J (1992) Carbon isotope fractionation between calcite, graphite and CO_2: an experimental study. Contrib Miner Petrol 112:35–45. doi:10.1007/BF00310954

Strens RGJ (1965) The graphite deposit of Seathwaite in Borrowdale, Cumberland. Geol Mag 102:393–406

Sunagawa I (1987) Morphology of minerals. In: Sunagawa I (ed) Morphology of crystals, part B. Terra, Tokyo, pp 509–587

Sunagawa I (2005) Crystals: growth, morphology and perfection. Cambridge University Press, Cambridge

Tan PH, Dimovski S, Gogotsi Y (2004) Raman scattering of non-planar graphite: arched edges, polyhedral crystals, whiskers and cones. Philos Trans R Soc Lond A 362:2289–2310. doi:10.1098/rsta.2004.1442

Walton AG (1969) Nucleation in liquids and solutions. In: Zettlemoyer AC (ed) Nucleation. Marcel Dekker, New York

Ward JC (1876) The geology of the northern part of the English Lake District. Memoir of the Geological Survey of Great Britain. Quarter Sheet 101SE (England and Wales Sheet 29, Keswick)

Weis PL, Friedman I, Gleason JP (1981) The origin of epigenetic graphite: evidence from isotopes. Geochim Cosmochim Acta 45:2325–2332. doi:10.1016/0016-7037(81)90086-7

Wopenka B, Pasteris JD (1993) Structural characterization of kerogens to granulite-facies graphite: applicability of Raman microprobe spectroscopy. Am Mineral 78:533–557